Heart rate control using first- and second-order models during treadmill exercise

Hanjie Wang & Kenneth J. Hunt

Published online: 16 Sep 2021.

Submit your article to this journal ⬈

View related articles ⬈

View Crossmark data ⬈

Taylor & Francis
Taylor & Francis Group

Heart rate control using first- and second-order models during treadmill exercise

Hanjie Wang [ID] and Kenneth J. Hunt [ID]

Institute for Rehabilitation and Performance Technology, Division of Mechanical Engineering, Department of Engineering and Information Technology, Bern University of Applied Sciences, Burgdorf, Switzerland

ABSTRACT

Heart rate control using first- and second-order models was compared using a novel control design strategy which shapes the input sensitivity function. Ten participants performed two feedback control test series on a treadmill with square wave and constant references. Using a repeated measures, counterbalanced study design, each series compared controllers C1 and C2 based on first- and second-order models, respectively. In the first series, tracking accuracy root-mean-square tracking error (RMSE) was not significantly lower for C2: 2.59 bpm vs. 2.69 bpm (mean, C1 vs. C2), $p = 0.79$. But average control signal power was significantly higher for C2: $11.29 \times 10^{-4}\,\mathrm{m^2/s^2}$ vs. $27.91 \times 10^{-4}\,\mathrm{m^2/s^2}$, $p = 3.1 \times 10^{-10}$. In the second series, RMSE was also not significantly lower for C2: 1.99 bpm vs. 1.94 bpm, $p = 0.39$; but average control signal power was again significantly higher for C2: $2.20 \times 10^{-4}\,\mathrm{m^2/s^2}$ vs. $2.78 \times 10^{-4}\,\mathrm{m^2/s^2}$, $p = 0.045$. The results provide no evidence that controllers based on second-order models lead to better tracking accuracy, despite the finding that they are significantly more dynamic. Further investigation using a substantially larger sample size is warranted.

1. Background

Heart rate (HR) is widely used to characterize exercise intensity. Many training protocols to enhance and sustain cardiorespiratory fitness are designed based on HR (Riebe et al., 2018). Heart rate is used in this way in healthy individuals (Garber et al., 2011) and also in different patient populations (Mezzani et al., 2013; Riebe et al., 2018). To achieve a better cardiorespiratory training effect, high-intensity interval training (HIIT), which applies a changing target HR, shows advantages compared to training with a constant exercise intensity (systematic reviews: Ramos et al., 2015; Weston et al., 2014). This motivates the need to design feedback systems for robust and accurate control of HR to follow arbitrary reference profiles.

The fundamental challenges of HR control are to model the dynamics of HR response to changes in exercise intensity to a sufficient level of accuracy, and also to deal appropriately with disturbance effects caused by heart rate variability (HRV) (Hunt & Fankhauser, 2016). Different HR control approaches based on either linear time-invariant models or nonlinear models have been proposed. Using the nonlinear model proposed by Cheng et al. (2008), several controllers have been developed:

Asheghan and Míguez (2016) analyzed the stability of the nonlinear model, designed a nonlinear control system and tested its robustness by simulating the system response with perturbations on model parameters and model inputs; Ibeas et al. (2016) designed a linear state feedback controller and simulations indicated the system was stable but robustness was not good enough; Esmaeili et al. (2019) proposed a feedback linearization control method, and simulation showed the system to be stable despite some states being incorrectly identified; Girard et al. (2016) proposed a PID controller based on a linear model located in the middle of the bounds of the nonlinear model, and performed a series of simulations to tune the parameters of the controller; Nguyen and Yagoubi (2018) designed a nonlinear static output feedback controller, they studied performance and robustness by simulation, and tested the controller with one participant; Du and Du (2018) presented a probabilistic model-based control strategy.

These studies have several important limitations: there is a general absence of quantitative evaluation outcomes for assessment of controller performance, and they are mainly simulation based. But due to substantial

---

human-to-human differences in physiological response, proper evaluation requires systematic empirical study with appropriate sample sizes, i.e. number of participants (Hunt & Maurer, 2016); furthermore, these works focus on uncertainty in model structure and parameters, while neglecting the key issue of disturbances caused by heart rate variability.

Compared to the existing results on modelling and control of heart rate reviewed above, our own work has focussed on the problem of rejection of disturbances attributable to heart rate variability, by utilizing novel linear time-invariant designs that make key closed-loop frequency response characteristics transparent. To address the research question of the present study, an important theoretical extension of our existing approach was required, viz. derivation of the control design equations for the case of a second-order plant model.

In principle, nonlinear models have an advantage in modelling accuracy due to better representation of the nonlinear characteristics of HR response, which mainly consist of slowly drifting dynamics caused by physiological changes, and also due to the dependence of dynamics on the operating point. But from the perspective of feedback controller design, slowly changing dynamics, or variations dependent on operating point, can be effectively compensated by integral action and by the fundamental ability of feedback to reduce uncertainty. Hence, appropriate modelling of relatively more rapid and more significant dynamic components of HR response might have more influence on closed-loop control accuracy than modelling of nonlinear phenomena: a previous study showed that a certain nonlinear control strategy did not lead to any improvement in control accuracy when compared to a simple linear time-invariant controller (Hunt & Maurer, 2016).

Consistent with these observations, linear time-invariant approaches have been shown to provide accurate and robust HR control using studies with quantitative outcomes and substantial numbers of participants, e.g. Hunt and Gerber (2017) and Hunt et al. (2019). Furthermore, it has been suggested that the issue of rejection of HRV-related disturbances (see Hunt & Saengsuwan, 2018) is more important than parametric model uncertainty, thus leading to the proposal for a linear control design approach based on shaping of the closed-loop input sensitivity function (Hunt & Fankhauser, 2016).

In a previous study (Wang & Hunt, 2021), two kinds of linear time-invariant transfer function were employed to model the HR response to treadmill speed changes: a second-order case that separately modelled Phase I (fast) and Phase II (slower) HR dynamics, and a first-order model that combined both phases into a single exponential response. Statistical analysis showed that the second-order transfer functions achieved significant improvement in goodness-of-fit. Hence, it was hypothesized that controllers based on second-order models could be more dynamic, and therefore give more accurate heart rate control, than controllers based on first-order models.

This study aimed to investigate whether heart rate control design based on second-order models can achieve better tracking accuracy as a consequence of a more dynamic control signal when compared to controllers designed from first-order models. To meaningfully address this question, both theoretical and experimental contributions were required. Firstly, to make this investigation possible, an important theoretical contribution was derived: a novel control design strategy which shapes the input sensitivity gain to be a monotonically decreasing function of frequency based on first-order models, (Hunt & Fankhauser, 2016), was extended to encompass second-order models. Secondly, the experimental contribution was that a formal test series was carried out using a cohort of 10 human participants.

2. Materials and methods

2.1. Controller design

2.1.1. Control structure and nominal plant model

This study employed an output feedback control structure (Figure 1) consisting of a feedback compensator C that adjusts treadmill speed using the difference between the filtered reference signal and the measured HR, a nominal plant model P_o that describes the response of HR to changes in treadmill speed, and a reference prefilter C_{pf} that shapes the overall closed-loop reference tracking response.

The plant P_o is represented by the strictly proper transfer function

$$P_o(s) = \frac{B(s)}{A(s)} : u \mapsto y \qquad (1)$$

where A and B are polynomials in s, with A monic and $n_b < n_a$.

The compensator C is constrained at the outset to be a strictly proper transfer function and is written as

$$C(s) = \frac{G(s)}{H(s)} : e \mapsto u \qquad (2)$$

with H monic. The strictly proper requirement, viz. $n_g < n_h$, is imposed to ensure that the compensator gain rolls off to 0 at high frequency, i.e. $\lim_{\omega \to \infty} |C(j\omega)| = 0$.

In the present work, and in the preceding system identification study (Wang & Hunt, 2021), two forms for the nominal plant model P_o are considered: first order and
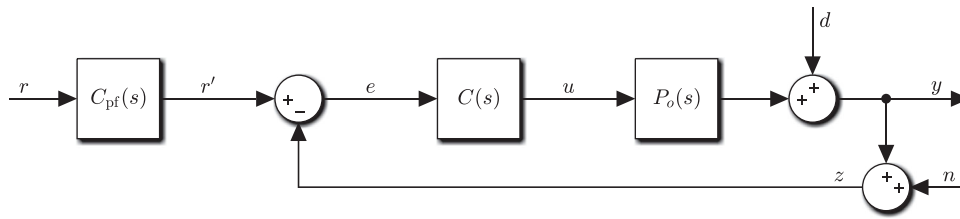
Figure 1. Block diagram of control structure for this study. $P_o(s)$ is the plant model, $C(s)$ is the feedback compensator, and $C_{\mathrm{pf}}(s)$ is a reference prefilter. The controlled variable (HR) is y, u is the control signal (treadmill speed target), d is a disturbance term than mainly comprises heart rate variability, and n models measurement noise. r is the reference/target HR signal and r' is the filtered HR reference.

second order, described respectively as

$$P_1(s) = \frac{k_1}{\tau_1 s + 1}, \tag{3}$$

where Phase I and Phase II HR dynamics are combined into a single time constant τ_1, and

$$P_2(s) = \frac{k_2}{(\tau_{21} s + 1)(\tau_{22} s + 1)} \tag{4}$$

with Phase I and Phase II HR dynamics represented using separate time constants τ_{21} and τ_{22}. In Equations (3) and (4), k_1 and k_2 are steady-state gains.

The polynomials A and B in the general plant transfer function description Equation (1), where A is required to be monic, can be identified for P_1 and P_2 as follows:

$$P_1: B(s) = b_0 = \frac{k_1}{\tau_1}, \quad A(s) = s + a_0 = s + \frac{1}{\tau_1} \tag{5}$$

$$P_2: B(s) = b_0 = \frac{k_2}{\tau_{21}\tau_{22}},$$

$$A(s) = s^2 + a_1 s + a_0 = \left(s + \frac{1}{\tau_{21}}\right)\left(s + \frac{1}{\tau_{22}}\right) \tag{6}$$

Corresponding to the two plant models, the transfer function of feedback compensator C also has two forms: one calculated from P_1 (denoted C_1), and one calculated from P_2 (denoted C_2), as described in the sequel.

2.1.2. Controller derivation: input-sensitivity shaping

Derivation of the controller structure and parameters is based upon the input sensitivity approach proposed by Hunt and Fankhauser (2016). That publication considered only the first-order model Equation (3), therefore it will be extended here to the second-order case, Equation (4).

The three principal closed-loop sensitivity functions for the feedback structure under consideration (Figure 1) are the input-sensitivity function U_o, the sensitivity function S_o, and the complementary sensitivity function T_o (Åström & Murray, 2008):

$$n, r', d \mapsto u: U_o(s) = \frac{C(s)}{1 + C(s)P_o(s)}, \tag{7}$$

$$d \mapsto y: S_o(s) = \frac{1}{1 + C(s)P_o(s)}, \tag{8}$$

$$n, r' \mapsto y: T_o(s) = \frac{C(s)P_o(s)}{1 + C(s)P_o(s)}. \tag{9}$$

The derivation process for the transfer function of compensator C is based on the requirement that the input-sensitivity function gain $|U_o|$ be a monotonically decreasing function of frequency, so that peaking is avoided. A special case of this requirement is when U_o is forced (shaped) to be a first-order transfer function (Hunt & Fankhauser, 2016).

Focusing now on the input-sensitivity function, employment of the polynomial forms for P_o and C, viz. Equations (1) and (2), leads to

$$U_o(s) = \frac{AG}{AH + BG} = \frac{AG}{\Phi} \tag{10}$$

where the closed-loop characteristic polynomial has been introduced as $\Phi = AH + BG$.

The compensator is now constrained in two ways: integral action is included by setting $H = sH'$, and a plant-pole cancellation strategy is employed by setting $G = AG'$. This results in

$$C(s) = \frac{AG'}{sH'} \tag{11}$$

and

$$\Phi = AsH' + BAG' = A\Phi' \Rightarrow \Phi' = sH' + BG'. \tag{12}$$

Following algebraic reasoning detailed in Hunt and Fankhauser (2016) that requires a unique solution to Equation (12) with C strictly proper, the degrees of polynomials G', H' and Φ' are $n_{g'} = 0$, $n_{h'} = n_a$ and $n_{\Phi'} = n_a + 1$, respectively, therefore $G' = g'_0$ (a constant).

It follows from Equation (10) that

$$U_o = \frac{A^2 G'}{A\Phi'} = \frac{Ag'_0}{\Phi'}. \tag{13}$$

To achieve further simplification, Φ' is set to include the factor A; but because $n_{\Phi'} = n_a + 1$, Φ' under this constraint can contain just one further pole and it must therefore have the form $\Phi' = A(s + p)$ where p is considered

a feedback design parameter. Developing Equation (13), the final form of the input-sensitivity function is then

$$U_o = \frac{g_0'}{(s+p)} \qquad (14)$$

which, as required at the outset, is a first-order transfer function: as such, $|U_o(j\omega)|$ must monotonically decrease with frequency towards the limit $\lim_{\omega \to \infty} |U_o(j\omega)| = 0$ and cannot have any peaking (in fact, this is a consequence of the strictly-proper constraint set on the compensator C). The design parameter p is seen to be the bandwidth of U_o.

Thus far, no constraint has been placed on the degree of the plant pole polynomial A, so that the above derivation is generic. But now the special cases of first- and second-order plants, $n_a = 1$ and $n_a = 2$, are considered: this amounts to finding the unique solution of the polynomial equation $\Phi' = sH' + BG'$, Equation (12), for each case.

The solution for a first-order plant was derived previously (Hunt & Fankhauser, 2016) and is merely summarized here. With $n_a = 1$, $n_{h'} = n_a = 1 \Rightarrow H' = s + h_0'$; and, in general, $G' = g_0'$. The unique solution for the unknown controller parameters is $g_0' = p/k_1$, $h_0' = p + 1/\tau_1$. Using Equations (5) and (11), the compensator for the first-order case is then

$$C_1(s) = \frac{AG'}{sH'} = \frac{\frac{p}{k_1}\left(s + \frac{1}{\tau_1}\right)}{s\left(s + p + \frac{1}{\tau_1}\right)}. \qquad (15)$$

Moving now to the second-order case, where $n_a = 2$, the structure of H' is seen to be $n_{h'} = n_a = 2 \Rightarrow H' = s^2 + h_1's + h_0'$. As before, $G' = g_0'$. Furthermore, $n_{\Phi'} = n_a + 1 = 3$. The polynomial equation from Equation (12), viz. $sH' + BG' = \Phi' = A(s+p)$, can now be solved by equating terms of like power on both sides to obtain the unique solution $g_0' = pa_0/b_0$ (from Equation (6), $a_0/b_0 = 1/k_2 \Rightarrow g_0' = p/k_2$), $h_0' = pa_1 + a_0$, $h_1' = p + a_1$. Finally, using the definitions of a_0 and a_1 from Equation (6), the compensator for the second-order case can be expressed as

$$C_2(s) = \frac{AG'}{sH'} = \frac{\frac{p}{k_2}\left(s^2 + \left(\frac{1}{\tau_{21}} + \frac{1}{\tau_{22}}\right)s + \frac{1}{\tau_{21}\tau_{22}}\right)}{s\left(s^2 + \left(p + \frac{1}{\tau_{21}} + \frac{1}{\tau_{22}}\right)s + p\left(\frac{1}{\tau_{21}} + \frac{1}{\tau_{22}}\right) + \frac{1}{\tau_{21}\tau_{22}}\right)}. \qquad (16)$$

2.1.3. Nominal models and controller calculation

The nominal model parameters for P_1 and P_2 were obtained from a previous identification study involving 11 participants (Wang & Hunt, 2021): 10 of these participants were included in the first test series described below (Section 2.2.2), and eight took part in the second series.

For the first test series, which used a square-wave reference profile, the nominal first- and second-order models for calculation of C_1 and C_2 were taken as the average of the 11 identified models in each case, so that a single C_1 compensator and a single C_2 compensator was applied to all 10 participants. The nominal P_1 and P_2 models were

$$P_1: k_1 = 28.57, \quad \tau_1 = 70.56,$$
$$P_2: k_2 = 24.70, \quad \tau_{21} = 18.60, \quad \tau_{22} = 37.95. \qquad (17)$$

The compensators C_1 and C_2 were calculated using Equations (15) and (16), and the sensitivity functions according to Equations (7), (8) and (9). The Bode magnitude plots of the resulting sensitivity functions are illustrated in Figure 2.

In the second test series, which involved eight participants, the compensators were calculated using each participant's individually identified first- and second-order models. The model parameters of P_1 and P_2 for each participant are listed in Table 1.

The reference prefilter C_{pf} was employed in the first test series to obtain a common overall closed-loop transfer function T_{cl} from reference signal r to controlled variable y (Figure 1), independent of the compensator and plant transfer functions. Following a procedure detailed elsewhere (Hunt & Fankhauser, 2016), T_{cl} was specified to be a standard second-order transfer function with critical damping and rise time of 150 s; the prefilter was then calculated as $C_{pf} = T_o^{-1}T_{cl}$, where T_o is the complementary sensitivity function, Equation (9). (Note: for the second test series, Section 2.2.2 below, the HR reference was constant, therefore the prefilter played no role in the outcomes.)

2.2. Experimental design

2.2.1. Participants

Ten healthy participants (8 males, 2 females) were recruited for this study, with age 30.1 years $\pm$ 9.9 years, body mass 77.4 ± 13.5 kg, and height 180.0 ± 11.4 cm (means $\pm$ standard deviations). The recruitment criteria were: regular exercisers (30 minutes each time, 3 times each week), nonsmokers, and free from cardiovascular disease or musculoskeletal complaints.

2.2.2. Test protocol

Two test series were performed: in the first, the heart rate reference was a square wave, while in the second it was constant. In each test series, each participant was tested once with compensator C_1 and once with C_2. To prevent order-of-presentation effects, the order of testing
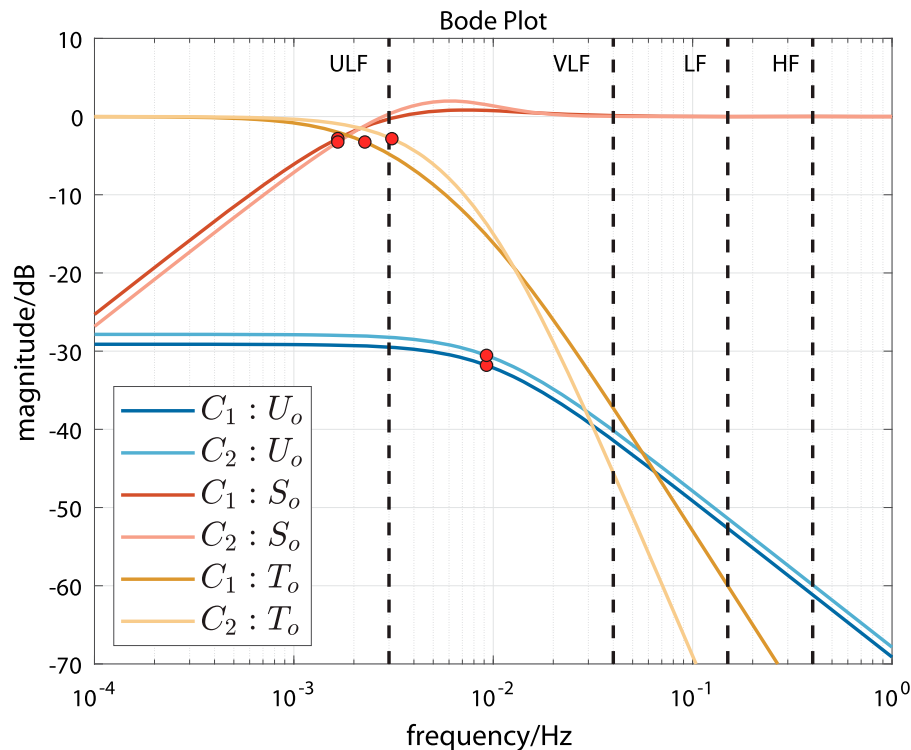
Figure 2. Closed-loop frequency responses for the first test series: input-sensitivity function (U_o), sensitivity function (S_o) and complementary sensitivity function (T_o); each function is plotted for compensators C_1 and C_2. Red dots mark the -3 dB cutoff frequency (bandwidth) for each transfer function. Vertical dashed lines distinguish four frequency bands of HRV (Shaffer & Ginsberg, 2017): ultra-low frequency (ULF, $\leq 0.00\overline{3}$ Hz), very-low frequency (VLF, $0.00\overline{3}$–0.04 Hz), low frequency (LF, 0.04–0.15 Hz) and high frequency (HF, 0.15–0.4 Hz).

with C_1 and C_2 was reversed for each participant based on the recruitment identification number, i.e. participant P01 was tested first with C_1, participant P02 with C_2, participant P03 with C_1, and so on. There was an interval of at least 48 hours between each test for each participant. Before each test, participants were instructed not to take intensive exercise for 24 hours, to avoid caffeine for 12 hours and not to have a large meal for 3 hours.

Each feedback test consisted of four phases: a 10-minute warm up, 10-minutes of rest, a 30-minute formal

measurement phase and a 10-minute cool down (Figure 3).

In the warm up phase, the speed of the treadmill was computed using the same compensator as for the formal measurement phase; the reference HR, denoted HR*, was set to a constant value HR_m corresponding to a HR between the ranges for moderate and vigorous exercise intensity (Riebe et al., 2018), calculated individually as $HR_m = 0.765 \times (220-\text{age})$ (except that, for participant P03, the factor was set to 0.7 to maintain an exercise intensity perceived as moderate).

In the formal measurement phase, the speed of the treadmill was continuously adjusted by the compensator (C_1 or C_2). The profiles for the reference heart rate signal HR* were defined as follows:

Table 1. Individual model parameters used in the second test series.

| ID	P_1		P_2		
	k_1	τ_1	k_2	τ_{21}	τ_{22}
P01	24.73	53.98	21.40	12.13	29.16
P02	31.49	67.16	26.70	27.80	27.80
P03	25.72	65.08	21.01	24.15	26.63
P04	19.73	65.87	17.77	9.68	45.82
P05	28.85	106.50	24.71	22.06	60.51
P08	36.61	69.64	33.33	10.71	49.45
P09	22.52	71.95	20.11	11.71	47.34
P10	30.67	66.18	25.28	20.24	25.44

Note: $n = 8$.
ID: participant identification number.
P_1: first-order model.
P_2: second-order model.

- The first series implemented a square-wave reference signal with mean HR_m, amplitude 10 bpm, and period 10 min (Figure 3(a)), i.e. HR* = $HR_m \pm 10$ bpm. The time interval between 295 s and 1795 s (totally 1500 s, 25 min) was used for calculation of the quantitative outcomes (below). The first five minutes of the formal evaluation phase allowed the HR of each participant to reach an initial steady state and hence were excluded from the evaluation period.
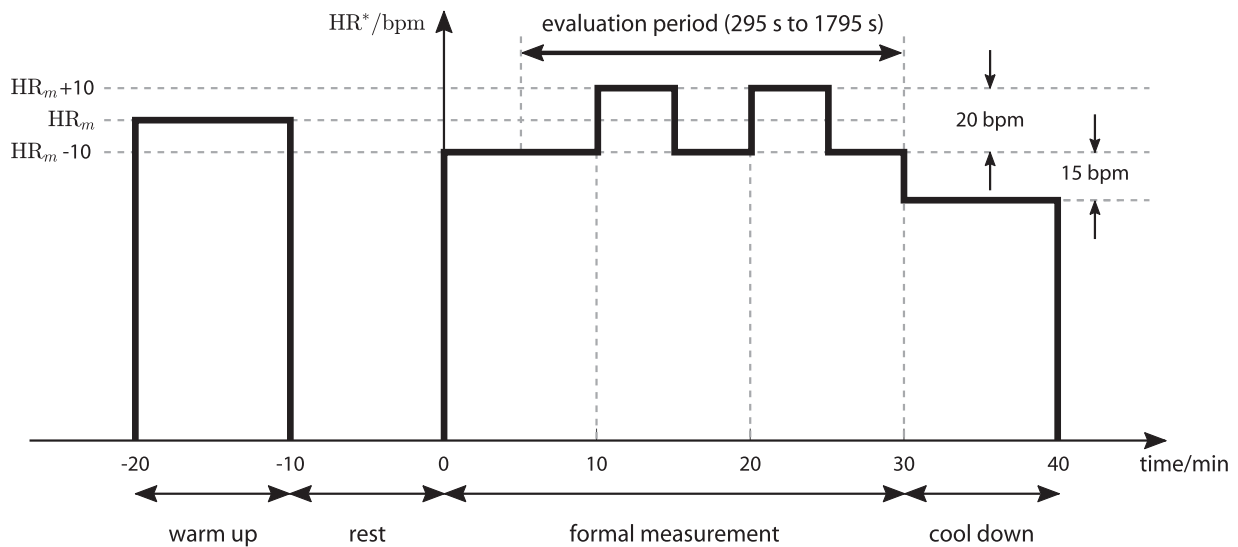
(a) Reference HR signal for first test series.
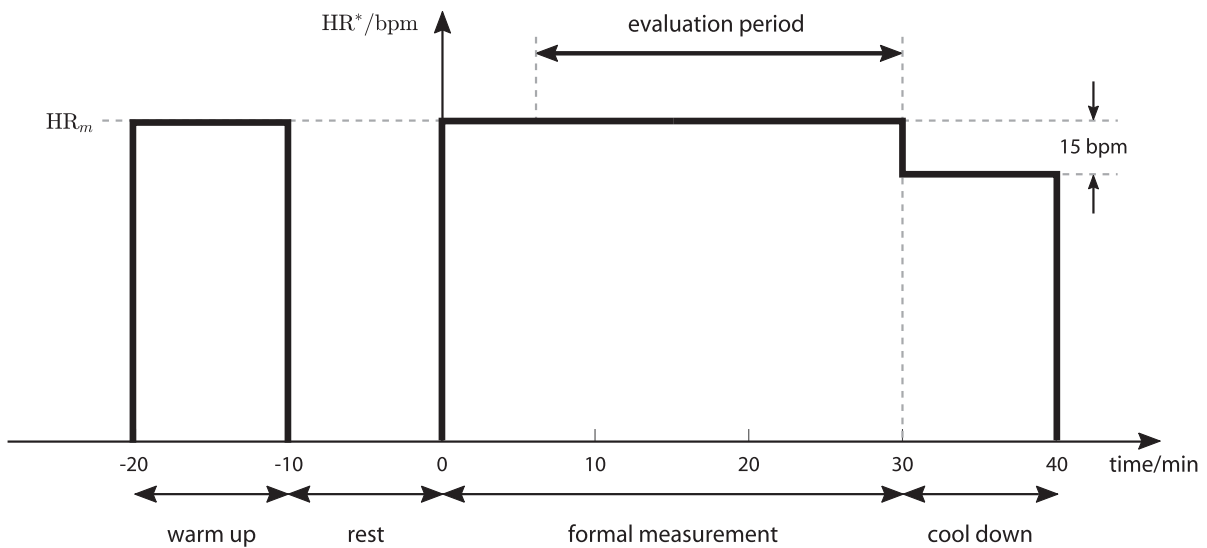
(b) Reference HR signal for second test series.

Figure 3. Test protocol with HR-reference profiles (HR*). Upper plot: profile of reference HR signal for the first test series (square wave). Lower plot: heart rate target for the second test series (constant). (a) Reference HR signal for first test series and (b) Reference HR signal for second test series.

- The second series applied a constant target HR equal to HR_m (Figure 3(b)). The start time of the evaluation period was the time when the measured HR first reached the target HR and was individually set. All the start times were in the range from 295 s to 495 s. The end time of the evaluation period was 1795 s for all participants.

In the cool down phase, the reference HR was kept constant for 10 min.

2.2.3. Equipment

All tests were carried out on a PC-controlled treadmill (model Venus, h/p/cosmos Sports & Medical GmbH, Germany; Figure 4). The control algorithm was implemented using real-time Simulink (The MathWorks, Inc., USA) running on the PC. Heart rate was measured by a chest strap (H10, Polar Electro Oy, Finland) and transferred to the PC through a wireless receiver module (Heart Rate Monitor Interface, Sparkfun Electronics, USA) at a rate of 1 Hz. The control algorithm ran at a sample rate of

0.2 Hz (sample interval 5 s) hence the HR measurement was downsampled by averaging every five consecutive values.

2.2.4. Evaluation outcome measures

The performance of compensators C_1 and C_2 was quantitatively evaluated by a tracking accuracy outcome and a control-signal intensity outcome. Tracking accuracy was evaluated by the root-mean-square error (RMSE, Equation (18)) between the HR measurement and the nominal (simulated) closed-loop HR response. The intensity of the control signal was assessed by the average power of changes in the treadmill speed (denoted $P_{\nabla u}$, Equation (19)):

$$\text{RMSE} = \sqrt{\frac{1}{N} \sum_{i=1}^{N} (\text{HR}_{\text{nom}}(i) - \text{HR}(i))^2}, \qquad (18)$$

$$P_{\nabla u} = \frac{1}{N-1} \sum_{i=2}^{N} (u(i) - u(i-1))^2. \qquad (19)$$

Here, HR_{nom} is the simulated closed-loop HR response and HR is the measured HR. u is the treadmill speed and N is the number of discrete sample instants over the evaluation period.

2.2.5. Statistics

Formal statistical analysis was carried out to test the hypotheses of this study, viz. that heart rate control design based on second-order models can achieve better tracking accuracy (RMSE for C2 lower than C1) as a consequence of a more dynamic control signal ($P_{\nabla u}$ higher for C2 than for C1) when compared to controllers designed from first-order models.

Prior to hypothesis testing, normality of differences between evaluation outcomes for C_1 and C_2 was assessed by a Kolmogorov-Smirnov test with Lilliefors correction. As all the differences were found not to significantly deviate from normality, paired one-sided t-tests were used with a significance level of 5% ($\alpha = 0.05$). Statistical analyzes were implemented using the Matlab Statistics and Machine Learning Toolbox (The Mathworks, Inc., USA).
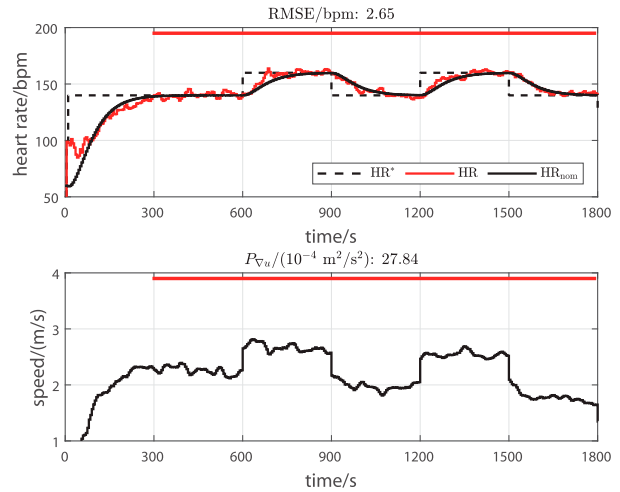
3. Results

Ten participants completed the first test series, but, due to non-availability of two participants, only eight of the 10
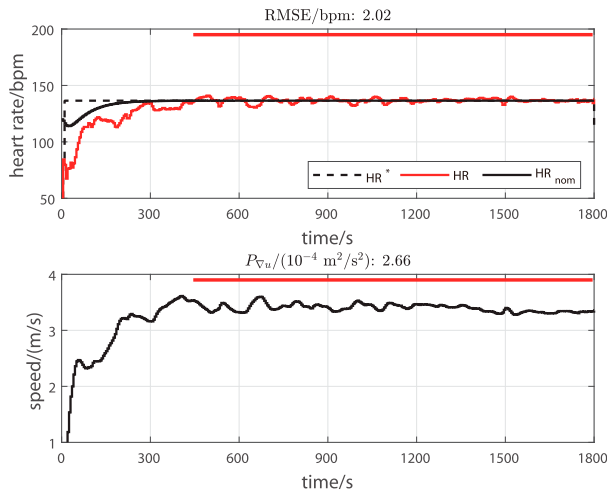

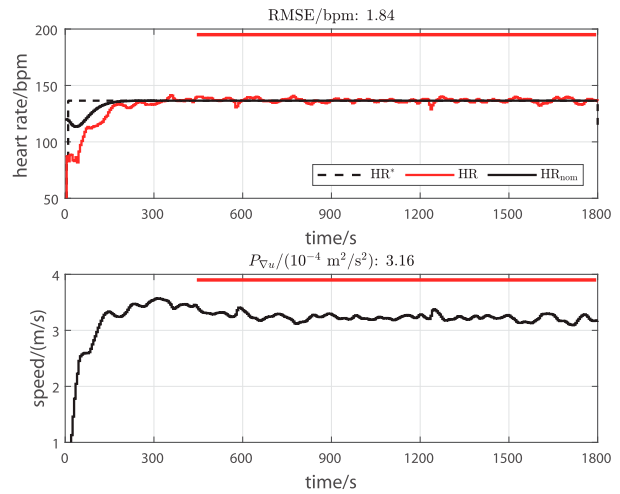**Figure 4.** The computer-controlled treadmill used in this study.
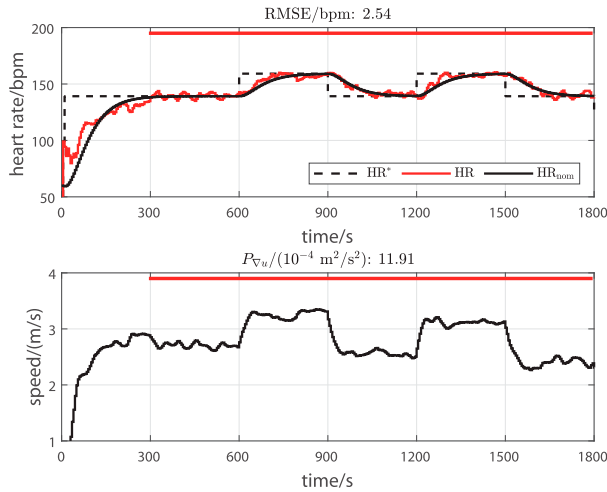
(a) First test series, C_1, P08.

(b) First test series, C_2, P09.

(c) Second test series, C_1, P03.

(d) Second test series, C_2, P03.

Figure 5. Measurements with RMSE closest to the mean in the two test series for the two compensator types. For each figure, the upper plot shows the reference heart rate signal (HR*, black dashed line), the measured heart rate (HR, red line) and the nominal (simulated) heart rate response (HR_nom, black line); the lower plots show the control signal, i.e. treadmill speed. The evaluation period for each measurement is denoted by a red horizontal bar. Participant number is denoted as P03, etc. (a) First test series, C_1, P08. (b) First test series, C_2, P09. (c) Second test series, C_1, P03 and (d) Second test series, C_2, P03.

Table 2. Sample properties for outcomes from C_1 and C_2 in the first test series and p-values for comparison of means (see also Figure 6(a,b)).

	mean ± SD		MD (95% CI)	
	C_1	C_2	C_2–C_1	p-value
RMSE/bpm	2.59 ± 0.50	2.69 ± 0.34	0.10 ($-\infty$, 0.32)	0.79
$P_{\nabla u}/(10^{-4}\,\mathrm{m^2/s^2})$	11.29 ± 1.65	27.91 ± 0.95	16.62 (15.49, ∞)	3.1×10^{-10}

Note: $n = 10$.
  C_1: compensator C_1.
  C_2: compensator C_2.
  SD: standard deviation.
  MD: mean difference of C_2–C_1.
  95% CI: confidence interval for the mean difference.
  p-values: paired one-sided t-tests.
  RMSE: root-mean-square error.
 $P_{\nabla u}$: average control signal power.
  bpm: beats per minute

completed the second series. Thus, a total of 36 datasets were available for analysis: 10 pairs of datasets (C1 and C2) for the first test series and eight pairs (C1 and C2) for the second series. To illustrate typical test results, the four measurements which had outcomes closest to the mean RMSE in each series and for each compensator type are provided (Figure 5).

In the first test series ($n = 10$), the tracking accuracy, as quantified by the root-mean-square tracking error (RMSE), was not significantly lower for C2 than for

C1: RMSE was 2.59 ± 0.50 bpm (mean $\pm$ standard deviation) vs. 2.69 ± 0.34 bpm, C1 vs. C2, $p = 0.79$ (Table 2, Figure 6(a)). On the other hand, average control signal power $P_{\nabla u}$ was found to be significantly higher for C2: $P_{\nabla u}$ was 11.29×10^{-4} m^2/s$^2 \pm 1.65 \times 10^{-4}$ m^2/s^2 vs. 27.91×10^{-4} m^2/s$^2 \pm 0.95 \times 10^{-4}$ m^2/s^2, C1 vs. C2, $p = 3.1 \times 10^{-10}$ (Table 2, Figure 6(b)).
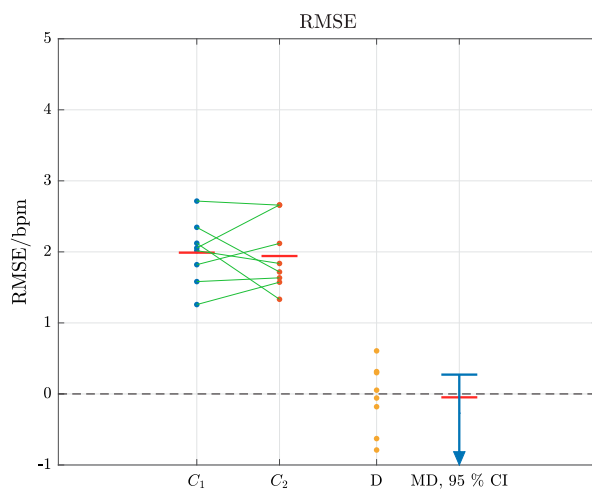
In the second test series ($n = 8$), RMSE for C2 was also found not to be significantly lower than for C1: RMSE was 1.99 ± 0.45 bpm vs. 1.94 ± 0.50 bpm, C1 vs. C2,
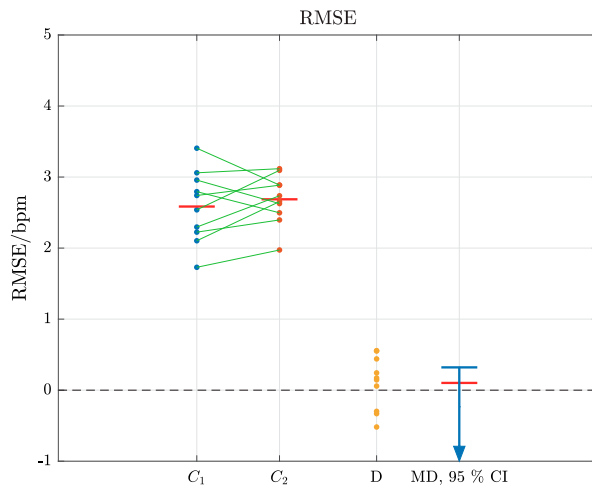
(a) RMSE for first test series.
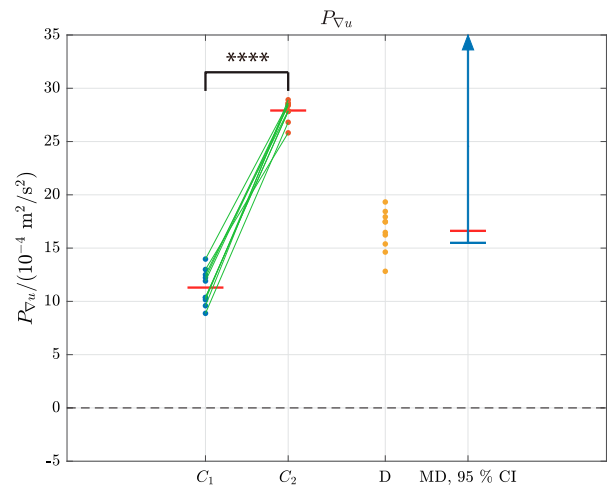
(b) $P_{\nabla u}$ for first test series.

(c) RMSE for second test series.
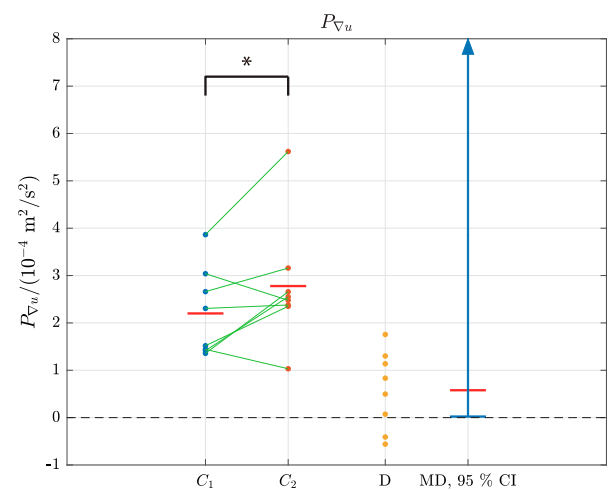
(d) $P_{\nabla u}$ for second test series.

Figure 6. Dispersion of samples for RMSE and $P_{\nabla u}$ from the two test series, with 10 sample pairs from the first test series (Figure 6(a,b)) and eight sample pairs from the second series (Figure 6(c,d)). In each figure, blue and red dots are the outcomes with compensators C_1 and C_2, respectively, green lines connect sample pairs for each participant, and red bars mark the sample means (given numerically in Tables 2 and 3). D denotes the difference between paired samples ($C_2 - C_1$) and MD (red horizontal bar) the mean difference. The 95% confidence intervals (CIs) are marked in blue. For $P_{\nabla u}$, the value 0 is outwith the 95% CI in both cases, indicating a significantly higher value for C_2 (the notation $\ast$ signifies $p < 0.05$ and $\ast\ast\ast\ast$ means $p < 0.0001$). For RMSE, the value 0 is inside the 95% CI in both cases, indicating that the values for C_2 are not significantly lower ($p > 0.05$). (a) RMSE for first test series. (b) $P_{\nabla u}$ for first test series. (c) RMSE for second test series and (d) $P_{\nabla u}$ for second test series.

Table 3. Sample properties for outcomes from C_1 and C_2 in the second test series and p-values for comparison of means (see also Figure 6(c,d)).

	mean ± SD		MD (95% CI)	
	C_1	C_2	$C_2 - C_1$	p-value
RMSE/bpm	1.99 ± 0.45	1.94 ± 0.50	−0.05 (−∞, 0.27)	0.39
$P_{\nabla u}/(10^{-4}\,\text{m}^2/\text{s}^2)$	2.20 ± 0.93	2.78 ± 1.30	0.58 (0.02, ∞)	0.045

Note: $n = 8$.
C_1: compensator C_1.
C_2: compensator C_2.
SD: standard deviation.
MD: mean difference of $C_2 - C_1$.
95% CI: confidence interval for the mean difference.
p-values: paired one-sided t-tests.
RMSE: root-mean-square error.
$P_{\nabla u}$: average control signal power.
bpm: beats per minute.

$p = 0.39$ (Table 3, Figure 6(c)); but $P_{\nabla u}$ was again significantly higher for C2, viz. $2.20 \times 10^{-4}\,\text{m}^2/\text{s}^2 \pm 0.93 \times 10^{-4}\,\text{m}^2/\text{s}^2$ vs. $2.78 \times 10^{-4}\,\text{m}^2/\text{s}^2 \pm 1.30 \times 10^{-4}\,\text{m}^2/\text{s}^2$, C1 vs. C2, $p = 0.045$ (Table 3, Figure 6(d)).

To graphically illustrate dispersion of the samples for both outcomes and for the two test series, sample pairs, their differences and the corresponding 95% confidence intervals (CIs) are provided (Figure 6). These plots allow the visual verification of the existence (or otherwise) of significant differences between the means: if the value 0 lies outwith the respective CI, a significant difference exists.

4. Discussion

This study aimed to investigate whether heart rate control design based on second-order models (C_2) can achieve better tracking accuracy – lower RMSE – as a consequence of a more dynamic control signal – higher average control signal power – when compared to controllers designed from first-order models (C_1). To facilitate this investigation, the input-sensitivity-shaping approach to feedback design was theoretically extended to cover second-order models.

A motivating factor for this hypothesis was the finding that second-order linear models, theoretically valid close to some nominal operating point, give significantly better goodness-of-fit (model fit and model RMSE) than first-order models in the approximation of heart rate dynamics (Wang & Hunt, 2021): with the inclusion of a faster response mode, controllers based on second-order models might be more dynamic and therefore more accurate.

It was found that C_2 controllers were indeed more dynamic, with significantly higher average control signal power $P_{\nabla u}$, but that this did not lead to significant improvements in tracking accuracy (RMSE was not lower

for C_2). This finding can in part be explained by the fundamental ability of feedback to reduce plant-model uncertainty (Åström & Murray, 2008), so that differences in closed-loop control performance are likely to be more difficult to detect empirically than differences in open-loop model fidelity.

Insight into the observed closed-loop outcomes can be obtained by examining the frequency responses of the various closed-loop sensitivity functions (Figure 2). The input sensitivity function U_o, which is the transfer function from the HRV disturbance term d to the control signal u, has a higher gain for C_2 than for C_1 across the whole frequency range, consistent with the more dynamic behaviour and significantly higher control signal power $P_{\nabla u}$ for C_2 that was observed.

The sensitivity function S_o, which is the transfer function between d and the controlled output y (HR), displays more nuanced behaviour: the gain of S_o is lower for C_2 over most of the ULF range but then becomes higher for C_2 at the higher end of the ULF band and over about half of the VLF range. Most significantly, the gain of S_o has a much higher peak for C_2 than for C_1. Thus, C_2 will better attenuate ultra-low-frequency disturbances, but it will more strongly amplify disturbances in the VLF band where $|S_o| > 1$. Further work on comparing C_1 and C_2 controllers should strive to balance these potentially confounding frequency response characteristics.

A further factor to be considered regarding the control structure, and which is relevant to the first test series, relates to design of the reference prefilter C_{pf}. It transpired that, for C_2, the prefilter transfer function was non-proper, thus leading to instantaneous increases in the control signal u in response to step changes in the reference r: see Figure 5(b), lower plot. In contrast, C_{pf} for the C_1 case was proper, giving smooth changes in u (Figure 5(a), lower plot). In the first series of tests, these differences in C_{pf} design may have tended to exaggerate the higher mean $P_{\nabla u}$ observed with C_2. Since the reference signal r was constant during the second test series, the design of C_{pf} did not influence the outcomes in this series, where significantly higher control signal power was again observed.

A limitation of the present study, and a further contributing factor in regard to the inconclusive RMSE outcome, was the low number of participants included. Here, there were 10 participants in the first series and eight of those completed the second series, whereas the open-loop modelling comparison (Wang & Hunt, 2021) had 22 pairs of goodness-of-fit outcomes and was strongly statistically powered (there were large effect sizes and p-values on the order of 10^{-10}). These considerations, in particular the relative difficulty of detecting differences in RMSE in closed-loop vs. open-loop scenarios, point

to the need for further investigation using substantially larger sample sizes.

5. Conclusions

The results provide no evidence that controllers based on second-order models lead to better tracking accuracy, despite the finding that they are significantly more dynamic. To explore this outcome in more detail, further investigation using a more carefully balanced control design and a substantially larger sample size is warranted.

Authors' contributions

KH and HW designed the study. HW did the data acquisition. HW and KH contributed to the analysis and interpretation of the data. HW wrote the manuscript and KH revised it critically for important intellectual content. Both authors read and approved the final manuscript.

Data availability statement

The data that support the findings of this study are available from the corresponding author, HW, upon reasonable request.

Disclosure statement

No potential conflict of interest was reported by the author(s).

Ethics approval

This research was performed in accordance with the Declaration of Helsinki. The study was reviewed and approved by the Ethics Committee of the Swiss Canton of Bern (Ref. 2019-02184). All participants provided written, informed consent.

ORCID

Hanjie Wang http://orcid.org/0000-0003-3505-3447
Kenneth J. Hunt http://orcid.org/0000-0002-6521-9455

References

Asheghan, M. M., & Míguez, J. (2016). Stability analysis and robust control of heart beat rate during treadmill exercise. *Automatica*, *63*, 311–320. https://doi.org/10.1016/j.automatica.2015.10.027

Åström, K. J., & Murray, R. M (2008). *Feedback systems*. Princeton University Press.

Cheng, T. M., Savkin, A. V., Celler, B. G., Su, S. W., & Wang, L. (2008). Nonlinear modeling and control of human heart rate response during exercise with various work load intensities. *IEEE Transactions on Biomedical Engineering*, *55*(11), 2499–2508. https://doi.org/10.1109/TBME.2008.2001131

Du, Y., & Du, D. (2018). Robust control design of heart rate response during treadmill exercise under parametric uncertainty. In *2018 40th Annual international conference of the IEEE engineering in medicine and biology society (EMBC)* (pp. 5830–5833). IEEE. https://doi.org/10.1109/EMBC.2018.8513520

Esmaeili, A., Ibeas, A., Ibrir, S., & Balaguer, P. (2019). Joint parameter-state estimation-based control of heart rate during treadmill exercise. In *2019 24th IEEE international conference on emerging technologies and factory automation (ETFA)* (pp. 1485–1488). IEEE. https://doi.org/10.1109/ETFA.2019.8869432

Garber, C. E., Blissmer, B., Deschenes, M. R., Franklin, B. A., Lamonte, M. J., Lee, I. M., Nieman, C., & Swain, D. P. (2011). Quantity and quality of exercise for developing and maintaining cardiorespiratory, musculoskeletal, and neuromotor fitness in apparently healthy adults. *Medicine and Science in Sports and Exercise*, *43*(7), 1334–1359. https://doi.org/10.1249/MSS.0b013e318213fefb

Girard, C., Ibeas, A., Vilanova, R., & Esmaeili, A. (2016). Robust discrete-time linear control of heart rate during treadmill exercise. In *2016 24th Iranian conference on electrical engineering (ICEE)* (pp. 1113–1118). IEEE. https://doi.org/10.1109/IranianCEE.2016.7585688

Hunt, K. J., & Fankhauser, S. E. (2016). Heart rate control during treadmill exercise using input-sensitivity shaping for disturbance rejection of very-low-frequency heart rate variability. *Biomedical Signal Processing and Control*, *30*, 31–42. https://doi.org/10.1016/j.bspc.2016.06.005

Hunt, K. J., & Gerber, S. (2017). A generalised stochastic optimal control formulation for heart rate regulation during treadmill exercise. *Systems Science & Control Engineering*, *5*(1), 481–494. https://doi.org/10.1080/21642583.2017.1398685

Hunt, K. J., & Maurer, R. R. (2016). Comparison of linear and nonlinear feedback control of heart rate for treadmill running. *Systems Science & Control Engineering*, *4*(1), 87–98. https://doi.org/10.1080/21642583.2016.1179139

Hunt, K. J., & Saengsuwan, J. (2018). Changes in heart rate variability with respect to exercise intensity and time during treadmill running. *BioMedical Engineering OnLine*, *17*(1), 128. https://doi.org/10.1186/s12938-018-0561-x

Hunt, K. J., Zahnd, A., & Grunder, R. (2019). A unified heart rate control approach for cycle ergometer and treadmill exercise. *Biomedical Signal Processing and Control*, *54*, Article ID 101601. https://doi.org/10.1016/j.bspc.2019.101601

Ibeas, A., Esmaeili, A., Herrera, J., & Zouari, F. (2016). Discrete-time observer-based state feedback control of heart rate during treadmill exercise. In *2016 20th International conference on system theory, control and computing (ICSTCC)* (pp. 537–542). IEEE. https://doi.org/10.1109/ICSTCC.2016.7790721

Mezzani, A., Hamm, L. F., Jones, A. M., McBride, P. E., Moholdt, T., Stone, J. A., Urhausen, A., & Williams, M. A. (2013). Aerobic exercise intensity assessment and prescription in cardiac rehabilitation. *European Journal of Preventive Cardiology*, *20*(3), 442–467. https://doi.org/10.1177/2047487312460484

Nguyen, A. T., & Yagoubi, M. (2018). Nonlinear static output feedback control for human heart rate during treadmill exercise. In *2018 IEEE conference on decision and control (CDC)* (pp. 3818–3823). IEEE. https://doi.org/10.1109/CDC.2018.8618887

Ramos, J. S., Dalleck, L. C., Tjonna, A. E., Beetham, K. S., & J. S. Coombes (2015). The impact of high-intensity interval training versus moderate-intensity continuous training on vascular function: a systematic review and meta-analysis. *Sports Medicine*, *45*, 679–692. https://doi.org/10.1007/s40279-015-0321-z

Riebe, D., Ehrman, J. K., Liguori, G., & Magal, M (Eds.). (2018). *ACSM's guidelines for exercise testing and prescription* (10th ed.). Wolters Kluwer.

Shaffer, F., & Ginsberg, J. P. (2017). An overview of heart rate variability metrics and norms. *Frontiers in Public Health*, *5*, 258. https://doi.org/10.3389/fpubh.2017.00258

Wang, H., & Hunt, K. J. (2021). Identification of heart rate dynamics during treadmill exercise: comparison of first- and second-order models. *BioMedical Engineering OnLine*, *20*, Article ID 37, 1–10. https://doi.org/10.1186/s12938-021-00875-7

Weston, M., Taylor, K. L., Batterham, A. M., & Hopkins, W. G. (2014). Effects of low-volume high-intensity interval training (HIT) on fitness in adults: a meta-analysis of controlled and non-controlled trials. *Sports Medicine*, *44*, 1005–1017. https://doi.org/10.1007/s40279-014-0180-z